Geomechanics and Engineering, *Vol. 33, No. 6 (2023) 553-565*
https://doi.org/10.12989/gae.2023.33.6.553

Experimental study of strength characteristics of reinforced broken rock mass

Yanxu Guo[1a], Qingsong Zhang*[1], Hongbo Wang[2], Rentai Liu[1], Xin Chen[1], Wenxin Li[3] and Lihai Zhang[4]

[1]*Geotechnical and Structural Engineering Research Center, Shandong University, Jinan 250061, China*
[2]*College of Civil Engineering and Architecture, Shandong University of Science and Technology, Qingdao 266590, China*
[3]*Key Laboratory of Mining Disaster Prevention and Control, Shandong University of Science and Technology, Qingdao 266590, China*
[4]*Department of Infrastructure Engineering, The University of Melbourne, VIC 3010, Australia*

(*Received July 25, 2021, Revised April 11, 2023, Accepted April 18, 2023*)

Abstract. As the structure of broken rock mass is complex, with obvious discontinuity and anisotropy, it is generally necessary to reinforce broken rock mass using grouting in underground construction. The purpose of this study is to experimentally investigate the mechanical properties of broken rock mass after grouting reinforcement with consideration of the characteristics of broken rock mass (i.e., degree of fragmentation and shape) and a range of reinforcement methods such as relative strength ratio between the broken rock mass and cement-based grout stone body (λ), and volumetric block proportion (VBP) representing the volumetric ratio of broken rock mass and the overall cement grout-broken rock mass mixture after the reinforcement. The experimental results show that the strength and deformation of the reinforced broken rock mass is largely determined by relative strength ratio (λ) and VBP. In addition, the enhancement in compressive strength by grouting is more obvious for broken rock mass with spherical shape under a relatively high strength ratio (e.g., λ=2.0), whereas the shape of rock mass has little influence when the strength ratio is low (e.g., λ=0.1). Importantly, the results indicate that columnar splitting failure and inclined shear failure are two typical failure modes of broken rock mass with grouting reinforcement.

Keywords: broken rock mass; compressive strength; degree of fragment; failure modes; grouting reinforcement; volumetric block proportion

1. Introduction

Broken rock mass is a commonly unfavorable geological condition in underground engineering, but is commonly found in geological structures such as fault fracture zone (Mahdevari and Moarefvand 2018, Mahdevari *et al.* 2020, Guo *et al.* 2020). During excavation, tunnels collapse easily due to the influence of broken rock mass. Pre-grouting reinforcement is required to improve the strength of broken rock mass and ensure the stability of surrounding rock (Guo *et al.* 2021). Therefore, the strength of reinforced broken rock mass is an important parameter in geotechnical engineering design (Kalender *et al.* 2014, Jin *et al.* 2018, Liu *et al.* 2018). However, because of the complexity of broken rock mass and its obvious heterogeneity and anisotropy, its reinforcement strength is affected by various factors. Given the influence of these factors on the strength characteristics of reinforced broken rock mass, their study for geotechnical engineering design is significant.

Broken rock masses can be grouped into uncemented broken rock mass and cemented broken rock mass, according to the different matrix cementation characteristics between rock blocks (Ozturk and Nasuf 2013, Afifipour and Moarefvand 2014). Existing studies on broken rock mass mainly focus on uncemented broken rock mass (such as soil-rock mixture) and seldom consider the interface cementation between the rock mass and the matrix (Xiao *et al.* 2019, Avşar 2020). While reinforced broken rock mass is cemented broken rock mass, their interface cementation may result in completely opposite mechanical properties to that of uncemented broken rock mass (Goodman and Ahlgren 2000, Huang *et al.* 2017, Shakeri *et al.* 2018, Ghareh *et al.* 2020). Therefore, it is necessary to study the influence of various factors on the mechanical properties of cemented broken rock. In addition, geological conditions that exist in nature are complex and diverse, and the relative strength ratios of broken rock mass and rock matrix is different. Current research mainly focuses on the medium within which the strength of broken rock mass is greater than the strength of the rock matrix, and seldom considers the condition of the strength of broken rock mass being less than that of the matrix (Kahraman and Alber 2006, Alber and Kahraman 2009, Ulusay and Erguler 2012, Liu *et al.* 2020, Zhou *et al.* 2020a).

At present, experimental research methods that examine the mechanical properties of broken rock mass are mainly divided into three categories. The first category is the in-situ test, such as that used by Savely (1990), Coli *et al.* (2011), and Liu *et al.* (2017). Although the in-situ test can truly reflect the mechanical properties of broken rock mass in the natural environment, it is time-consuming, laborious, costly,

*Corresponding author, Professor
E-mail: zhangqingsong@sdu.edu.cn
[a]Ph.D.
E-mail: guoyanxuguo@163.com

ISSN: 2005-307X (Print), 2092-6219 (Online)

and only a few tests can be performed. Consequently, the test results are likely to have greater uncertainty. The second category of methods is laboratory testing of field-cored specimens, such as that used by Kahraman and Alber (2006), Alber and Kahraman (2009), and Sonmez *et al.* (2016). However, in practical engineering, due to factors such as geological genesis, rock structure property, and sampling disturbance, it is difficult to obtain complete core samples. In addition, due to the uncertainty of core location and massive dispersion of broken rock mass, it is difficult to obtain representative core samples, so the mechanical parameters obtained may not be representative. The third category of methods is laboratory testing of artificial samples. This category of methods is used to simulate a core sample of natural broken rock whose mechanical properties are then tested in a laboratory. Such methods are used by Li *et al.* (2013), Mahdevari and Moarefvand (2018), and Sagong *et al.* (2020). The artificial sample method is simple to operate, involves variables that are easy to control, will not cause test errors that can arise from excessive factors, and has strong test repeatability. It is an effective method for studying the factors that influence strength characteristics of broken rock mass.

To effectively control for the uncertainty of strength and shape of broken rock mass, this study adopted the method of laboratory testing of artificial samples, used cement mortar to prepare test blocks of different strengths, volumes, and shapes to simulate broken rock mass, and mixed the mortar specimens with cement slurry to produce broken rock mass reinforcement samples. Mechanical tests were then carried out on the reinforced samples to study the influence of relative strength ratio, volumetric block proportion, degree of fragmentation and shape of the rock block on the strength of reinforced broken rock mass. These tests revealed mechanical properties of reinforced broken rock mass varied under different influencing factors.

2. Experimental study on strength characteristics of reinforced broken rock mass

2.1 Experimental methodology

The purpose of the study is to examine the influence of relative strength ratio, volumetric block proportion, degree of fragmentation, and shape of different rock blocks on the strength of reinforced broken rock mass. The experimental process undertaken is outlined as follows (also see flow chart in Fig. 1).

(1) To simulate the different strengths of reinforced broken rock mass, we mixed cement, standard sand, bentonite and water in different ratios by weight to fabricate mortar specimens of various strengths. To test the strength (28d) of mortar specimens with different material ratios, material ratios of mortar specimens that simulate broken rock mass were selected.

(2) Based on selected test results, and according to the purpose of experimental research, mortar specimens of different strengths, volumes, and shapes were made using the molds shown in Fig. 2. After the mortar specimens had

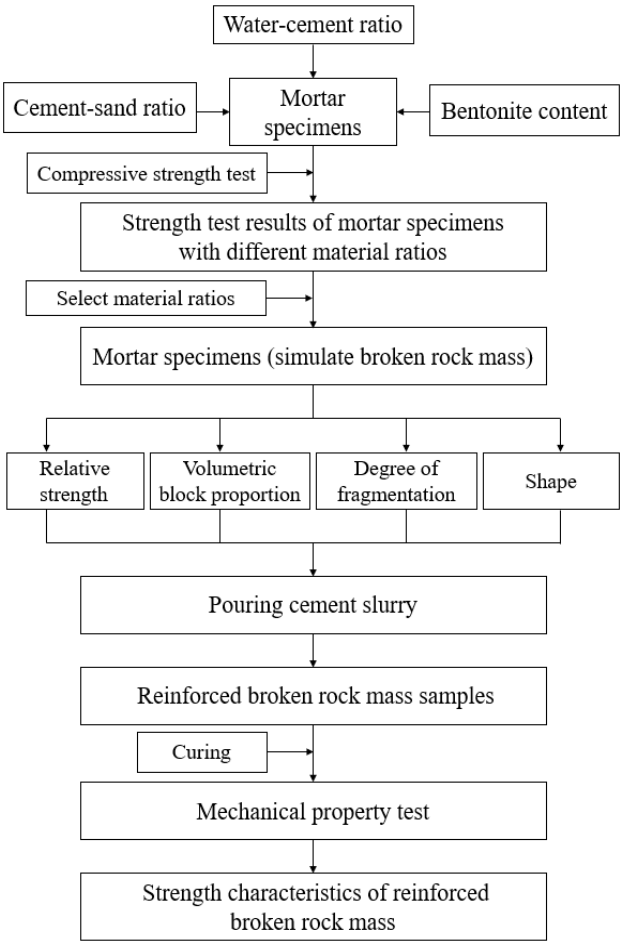

Fig. 1 Flow chart of the experimental process

Fig. 2 Molds for mortar specimens

formed, they were taken out of the molds and placed into cylindrical molds with cement slurry (Fig. 3) to make standard reinforced cylinder samples (including mortar specimens). When the samples reached curing time (28d), their uniaxial compressive strength was tested.

2.2 Test materials

At present, artificial rock blocks that simulate broken rock masses mainly consist primarily of cement, sand, plaster of Paris, among others, supplemented by bentonite

Table 1 The chemical composition of cement used in the test

Cement	SiO_2	CaO	Al_2O_3	MgO	SO_3	Fe_2O_3	K_2O	Na_2O	TiO_2	Others
PO 42.5	21.65%	54.06%	9.15%	3.90%	3.62%	2.85%	0.66%	0.24%	0.49%	3.38%

Table 2 The physical parameters of sand samples used in the test

Sand Sample Number	Sand Particle Size (mm)	D_{15} (mm)	ρ_{dmax} (g/cm^3)	ρ_{dmin} (g/cm^3)	e_{min}	e_{max}
1	0.08-0.315	0.118	1.614	1.424	0.636	0.861
2	0.315-0.63	0.362	1.671	1.489	0.578	0.780
3	0.63-1.25	0.723	1.686	1.493	0.571	0.775
4	1.25-2.5	1.438	1.706	1.539	0.554	0.748

Table 3 The chemical composition of bentonite used in the test

Composition	SiO_2	Al_2O_3	Fe_2O_3	MgO	TiO_2	CaO	K_2O	Na_2O	Loss on ignition
Content	63.66%	16.64%	4.93%	1.69%	0.59%	0.88%	1.37%	1.02%	9.22%

Table 4 Test mold parameters

Type	Cube 1, l	Sphere, r	Equilateral triangular prism		Cube 2, l	Cube 3, l
			a	h		
Parameter (mm)	15	12.4	30.4	20	20	30

Note: l = side length of cube; r = radius of sphere; a = bottom side length of equilateral triangular prism; h = height of equilateral triangular prism; The sphere mold, regular triangular prism mold and cube 2 mold have the same volume

Fig. 3 Molds for standard reinforced cylinder sample

and fly ash (Asadizadeh *et al*. 2019, Shaunik and Singh 2019, Zhang *et al*. 2019, Zhou *et al*. 2020b, Fereshtenejad *et al.* 2021). To simulate broken rock mass of different strengths, we mixed cement, standard sand, bentonite and water in different ratios by weight to fabricate mortar specimens of various strengths.

2.2.1 Ordinary Portland cement

The test cement is 42.5 Portland cement, and its quality conforms to the standard of <Common Portland Cement> (GB175-2007). The chemical composition of the test cement is shown in Table 1.

2.2.2 Standard sand

The test sand was China ISO standard sand, which is the Chinese standard (GSB08-1337) for testing cement strength. The particle size range of standard sand used in the test was 0.08-2.5 mm. Standard sand was screened by a standard vibrating screen machine, and four particle sizes of 0.08-0.315 mm, 0.315-0.63 mm, 0.63-1.25 mm, and 1.25-2.5 mm were retained. The physical parameters of each sand sample are shown in Table 2.

2.2.3 Bentonite

Bentonite is Na-bentonite, with montmorillonite as its main mineral constituent. Its main chemical compositions are SiO_2, Al_2O_3, and a small amount of Fe_2O_3, MnO_2, MgO, CaO, K_2O, Na_2O, TiO_2. Its specific chemical composition is shown in Table 3.

2.3 Testing specimens

Cube, sphere, and equilateral triangular prism molds (Fig. 2) respectively were made according to specific mold parameters as shown in Table 4. Plexiglass molds (Fig. 3) with an internal dimension of 50×100 mm, were used to prepare the mortar specimens within standard reinforced cylinder samples for strength testing.

2.4 Artificially simulated broken rock mass

2.4.1 Material ratios

Water-cement ratio

To consider differences in strength and molding rate of mortar specimens after mixing cement slurry and standard sand, the water-cement ratios of the cement slurry in this test were 0.4:1, 0.5:1, 0.8:1, 1:1, and 1.5:1, respectively.

Cement-sand ratio

In this test, standard sand of four particle sizes of 0.08-

Table 5 Test design for making mortar specimens of different proportions

Type	Water-Cement ratio	Cement-Sand Ratio	Bentonite Content	Particle Size (mm)
1	0.4	1:1, 1:2, 1:3, 1:4	0%	0.08-0.315, 0.315-0.63, 0.63-1.25, 1.25-2.5
2	0.5	1:1, 1:2, 1:3, 1:4	0%	0.08-0.315, 0.315-0.63, 0.63-1.25, 1.25-2.5
3	0.8	1:1, 1:2, 1:3, 1:4	0%	0.08-0.315, 0.315-0.63, 0.63-1.25, 1.25-2.5
4	1.0	1:1, 1:2, 1:3, 1:4	0%, 10%, 20%, 30%, 40%	0.08-0.315, 0.315-0.63, 0.63-1.25, 1.25-2.5
5	1.5	1:1, 1:2, 1:3, 1:4	0%, 10%, 20%, 30%, 40%	0.08-0.315, 0.315-0.63, 0.63-1.25, 1.25-2.5

Table 6 Material ratios and strengths of artificially simulated broken rock mass

Mortar Type	Water-Cement Ratio	Cement-Sand Ratio	Bentonite Content	Particle Size (mm)	Compressive Strength (MPa)	Relative Strength Ratio
M1	0.4	1:1	0%	0.08~0.315	42.85	2.5
M2	0.5	1:1	0%	0.315~0.63	34.28	2.0
M3	0.8	1:2	0%	0.315~0.63	20.57	1.2
M4	0.8	1:2	0%	0.63~1.25	13.71	0.8
M5	1.0	1:4	0%	0.315~0.63	8.57	0.5
M6	1.0	1:1	30%	0.63~1.25	5.14	0.3
M7	1.5	1:4	30%	0.315~0.63	1.71	0.1

Note: Relative strength ratio will be defined below

Table 7 Types of artificially simulated broken rock mass

Broken Rock Mass Type			Shape	Mortar Type
BRMC	BRMC1	BRMC11	Cub 1	M2
		BRMC12	Cub 1	M7
	BRMC2	BRMC21	Cub 2	M2
		BRMC22	Cub 2	M7
	BRMC3	BRMC31	Cub 3	M1
		BRMC32	Cub 3	M2
		BRMC33	Cub 3	M3
		BRMC34	Cub 3	M4
		BRMC35	Cub 3	M5
		BRMC36	Cub 3	M6
		BRMC37	Cub 3	M7
BRMS		BRMS1	Sphere	M2
		BRMS2	Sphere	M7
BRME		BRME1	Equilateral triangular prism	M2
		BRME2	Equilateral triangular prism	M7

0.315 mm, 0.315-0.63 mm, 0.63-1.25 mm, and 1.25-2.5 mm was used. The cement-sand ratios were 1:1, 1:2, 1:3, and 1:4, respectively.

Bentonite content

In this test, the contents of bentonite were 0%, 10%, 20%, 30%, and 40%, respectively.

2.4.2 Test design

To identify the material ratios of different mortar specimen strengths and obtain more test data for selection, a comprehensive test was designed. By considering different water-cement ratios, cement-sand ratios and bentonite content, mortar specimens of different strengths (cube 3) were prepared. The purpose of choosing water-cement ratios of 0.4:1, 0.5:1, 0.8:1 was to prepare high-strength mortar specimens; therefore, bentonite was not added. The purpose of choosing water-cement ratios of 1:1 and 1.5:1 was to prepare low-strength mortar specimens, so the addition of different bentonite contents was considered. The specific test design is shown in Table 5.

2.4.3 Selection of artificially simulated broken rock mass

Table 8 Test design

Volumetric Block Proportion	27.5%						
Broken Rock Mass Type	BRMC31	BRMC32	BRMC33	BRMC34	BRMC35	BRMC36	BRMC37
Relative Strength ratio (λ)	2.5	2.0	1.2	0.8	0.5	0.3	0.1

Table 9 Test design

Broken Rock Mass Type	Volumetric Block Proportion	Broken Rock Mass Type	Volumetric Block Proportion
BRME1	4.1%	BRME2	4.1%
	8.1%		8.1%
	12.2%		12.2%

Table 10 Test design

Volumetric Block Proportion	Broken Rock Mass Type	Volumetric block proportion	Broken Rock Mass Type
27.5%	BRMC32*2	27.5%	BRMC37*2
	BRMC11*8 and BRMC32*1		BRMC12*8 and BRMC37*1
	BRMC11*16		BRMC12*16

As mentioned above, the mortar specimens were mixed with cement slurry. Therefore, cement slurry of smaller water-cement ratio should be selected: we found that if the water-cement ratio was too high, it would cause precipitation of mortar specimens; if the water-cement ratio was too small, slurry fluidity would be lost, and the cement slurry would not sit perfectly with the mortar specimens, resulting in voids in the reinforced sample. After many tests, it was determined that the water-cement ratio was 0.5 and the uniaxial compressive strength was 17.14 MPa.

Rocks in nature are complex and diverse and of different strengths. According to Johnston and Choi (1986), Agustawijaya (2007), Shen (2014), Gerolymatou and Triantafyllidis (2016), Zhou *et al.* (2019), and Zhang *et al.* (2020), the material ratios and strengths of selected simulated broken rock mass are shown in Table 6. In addition, although rocks have various shapes, they can still be described by regular geometric shapes based on some simplifications (Brown 1981). Table 7 shows the types of mortar specimens selected in this study to simulate broken rock mass.

2.5 Experimental study on the influence of relative strength ratio on the strength of reinforced broken rock mass

Relative strength ratio (λ) is defined as the ratio of the strength of the mortar specimen to the strength of the cement-based grout stone body. To study the influence of relative strength ratio on the strength of reinforced broken rock mass, used the following types of broken rock mass: BRMC31, BRMC32, BRMC33, BRMC34, BRMC35, BRMC36, and BRMC37. The specific test design is shown in Table 8.

2.6 Experimental study on the influence of volumetric block proportion on the strength of reinforced broken rock mass

Volumetric block proportion (VBP) is defined as the volumetric ratio of mortar specimens and the overall cement grout-mortar specimens mixture after the reinforcement. BRME1 and BRME2 were used to study the influence of volumetric block proportion on the strength of reinforced broken rock mass under different relative strength ratios. The specific test design is shown in Table 9.

2.7 Experimental study on the influence of degree of fragmentation on the strength of reinforced broken rock mass

BRMC11, BRMC12, BRMC32, and BRMC37 types of broken rock mass were used to study the influence of degree of fragmentation on the strength of reinforced broken rock mass under different relative strength ratios. The specific test design is shown in Table 10.

2.8 Experimental study on the influence of shape on the strength of reinforced broken rock mass

BRMC21, BRMC22, BRMS1, BRMS2, BRME1, and BRME2 types of broken rock mass were used to study the influence of shape (with the same volumetric block proportion) on the strength of reinforced broken rock mass under different relative strength ratios. The specific test design is shown in Table 11.

In addition, to better describe the influence of rock block shape on the reinforcement strength, the concept of sphericity was introduced to quantitatively characterize the rock block shape (Romanova *et al*. 2009, Kim *et al.* 2016)

$$S^* = \frac{S_s}{S_p} \tag{1}$$

where S^* is the sphericity of the rock block, S_s is the surface area of the sphere equal in volume to the rock block, and S_p is the surface area of the rock block.

Table 11 Test design

Volumetric Block Proportion	Broken Rock Mass Type	Volumetric Block Proportion	Broken Rock Mass Type
27.5%	BRMS1	27.5%	BRMS2
	BRMC21		BRMC22
	BRME1		BRME2

Table 12 Sphericity of different rock block shapes

Shape	Sphericity
Sphere	1
Cube	0.806
Equilateral triangular prism	0.737

Using Eq. (1), the sphericity values of the different shapes of rock blocks in this study were obtained, as shown in Table 12.

3. Experimental results and analysis of strength characteristics of reinforced broken rock mass

3.1 The influence of relative strength ratio on the strength of reinforced broken rock mass

3.1.1 Mode of reinforcement failure

The mode of reinforcement failure reflects the strength characteristics of the broken rock mass and the overall mechanical properties of the reinforcement. As shown in Fig. 4, the uniaxial compression test results indicated that failure of reinforced broken rock mass presents in two typical failure modes depending on the different strength of the internal rock blocks under unconfined pressure. When the strength of the internal blocks is higher than the strength of the cement-based grout stone body, the sample displays columnar splitting. A failure surface is generated and develops along the interface, and one or more cracks penetrate the entire reinforcement sample at the edge. When the strength of the internal blocks is lower than the strength of the cement-based grout stone body, the sample displays inclined shear failure. Surface failure is generated and develops in the internal rock blocks, and the whole reinforced sample is cut obliquely.

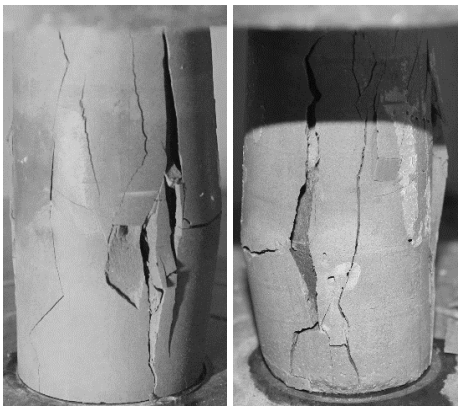

(a) Columnar splitting failure

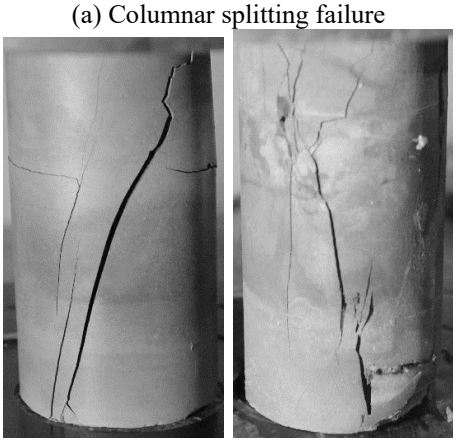

(b) Inclined shear failure

Fig. 4 Failure modes of reinforced samples

Fig. 5 shows the uniaxial compression test results of the reinforced samples containing mortar specimens of different relative strength ratios. It can be seen from Fig. 5 that the failure modes of samples (a), (b), and (c) are basically the same: columnar splitting failure. The integrity of these mortar specimens was good, the failure surface developed tortuously around the mortar specimens, and failure was mainly interface failure. The reasons for this failure are as follows: compared with the strength of mortar specimens and cement-based grout stone body, the strength of the interface between the mortar specimens and cement-based grout stone body is weak. Under unconfined pressure, interface strength controls the generation and development of cracks. With gradual increase in pressure, cracks gradually run through the whole sample. The failure modes of samples (f) and (g) are basically the same: inclined shear failure. The cracks are generated inside the mortar specimens, and failure surface occurs inside the mortar specimens instead of at the interface. The reasons are as follows: the tensile strength of the specimen is less than the tensile strength of the cement-based grout stone body and the interface strength, and it becomes an important factor to control the failure mode of the reinforced sample. The external load forces the first crack in the specimen. With continuous increase in pressure, internal cracks in the specimen are accelerated, and inclined-shear cracks develop in the entire sample until the sample is finally destroyed. Samples (d) and (e) display both columnar splitting failure and inclined shear failure. The difference is that sample (d) is mainly interface failure, with small cracks in the specimens, while sample (e) displayed large inclined-shear cracks that ran through the whole sample. These results indicate that the compression failure of reinforced broken rock mass is a complicated process. When the strength of the mortar specimen is less than the strength of the cement-based grout stone body, the strength of the reinforced sample is affected both by the strength of the specimen and

(a) BRMC31 (b) BRMC32 (c) BRMC33 (d) BRMC34 (e) BRMC35 (f) BRMC36 (g) BRMC37

Fig. 5 Internal failure of reinforced samples

the strength of the interface. The irregularity of specimens will lead to stress concentration in the sample, resulting in the coexistence of interface failure and internal failure of the specimen (Binaree *et al.* 2020). In summary, the relative strength ratio between the mortar specimen and the cement-based grout stone body will change the internal load transfer of the reinforcement, resulting in different mechanical properties and affecting the generation and development of the failure surface, which in turn affect the overall strength of the reinforced sample.

3.1.2 Stress-strain curves

Fig. 6 shows the stress-strain curves of the reinforced samples of mortar specimens under different relative strength ratios, which indicate the following:

(1) The stress-strain curves corresponding to samples BRMC31, BRMC32, BRMC33, and BRMC34 are all bimodal. At the initial stage of loading, the stress increases slowly with the strain, then increases faster, which is a basically linear relationship. The reason for this may be that the sample is not completely in contact with the testing machine at the initial stage of loading, and there is a stable process of the contact surface between the sample and the machine. As the load continues to increase, the stress increases approximately linearly with the strain. At the stage before the peak, the increasing rate of stress with strain decreases gradually, showing plastic characteristics and reaching the first peak. The stress then decreases rapidly; when it reaches the first peak valley, the stress increases with strain and reaches the second peak. From λ=2.5 to λ=0.8, the strength of the second peak decreases gradually. The reason for this is that the strength of mortar specimens inside the sample is relatively high, and the specimens are located at the center of the sample. With increase in load, the skeleton support of the specimens strengthens the reinforced sample and increases its overall strength. When the stress reaches the second peak, the stress again decreases with increase in strain.

(2) The stress-strain curves corresponding to samples BRMC35, BRMC36, and BRMC37 are all unimodal. The stress-strain curve before peak strength is similar to the curve before the first peak for samples BRMC31, BRMC32, BRMC33, and BRMC34, and were in the compaction stabilization, linear elasticity, and plastic stages. Then, the stress on samples BRMC35, BRMC36, and BRMC37 decreased rapidly. The phenomenon of stress increasing with the strain (i.e., the second peak) did not present.

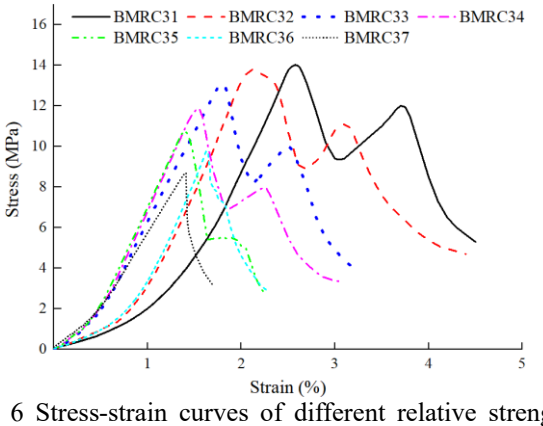

Fig. 6 Stress-strain curves of different relative strength ratios

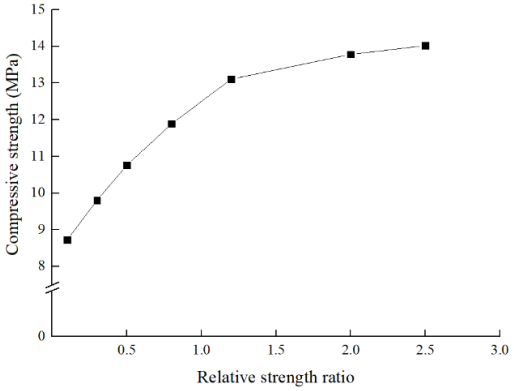

Fig. 7 The relationship between relative strength ratio and reinforcement strength

It can be seen from the stress-strain curves that the overall strength of the reinforced samples increases with increase in relative strength ratio, and the rate of increase has a gradually decreasing trend (Fig. 7). Although the curves are different in that they are bimodal or unimodal, the whole process of deformation of reinforced samples of different relative strength ratios under compression can still be divided into four stages: compaction stabilization stage, linear elastic stage, plastic stage and failure stage. The first three stages are basically the same. The difference lies in the influence of relative strength ratio on the overall strength of the reinforced sample in the failure stage.

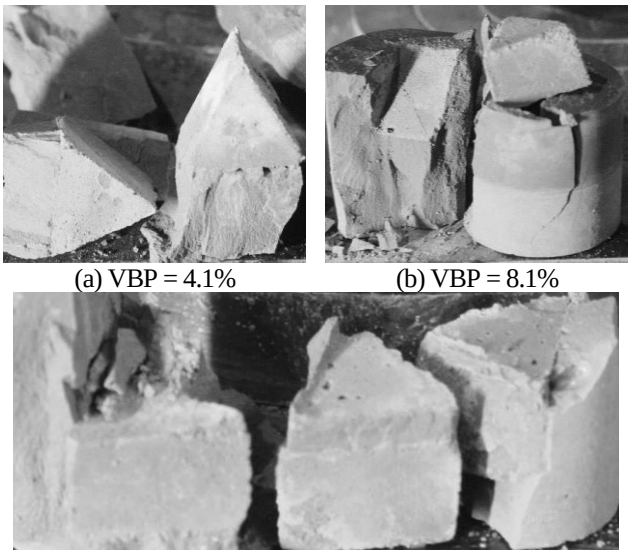

(a) VBP = 4.1% (b) VBP = 8.1%

(c) VBP = 12.2%

Fig. 8 Internal failure of reinforced samples with different volumetric block proportions (λ=2.0)

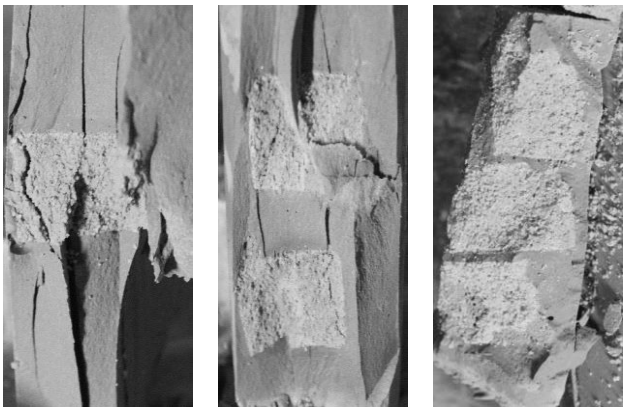

(a) VBP = 4.1% (b) VBP = 8.1% (c) VBP = 12.2%

Fig. 9 Internal failure of reinforced samples with different volumetric block proportions (λ=0.1)

3.2 The influence of volumetric block proportion on the strength of reinforced broken rock mass

3.2.1 Mode of reinforcement failure

The failure mode of the sample is similar to that shown in Fig. 4 and will not be described in detail. Fig. 8 shows the uniaxial compression test results of the reinforced samples (BRME1) of different volumetric block proportions. The integrity of the mortar specimens is good, and failure is mainly interface failure. Fig. 9 shows the uniaxial compression test results of reinforced samples (BRME2) of different volumetric block proportions. The cracks are generated inside the mortar specimens, which are completely destroyed.

3.2.2 Stress-strain curves

Fig. 10 shows the stress-strain curves of the reinforced samples of mortar specimens with different volumetric block proportions. The stress-strain curves (BMRE1) are all bimodal and similar to the above-mentioned stress-strain curve for BMRC32. The difference is that the second peak

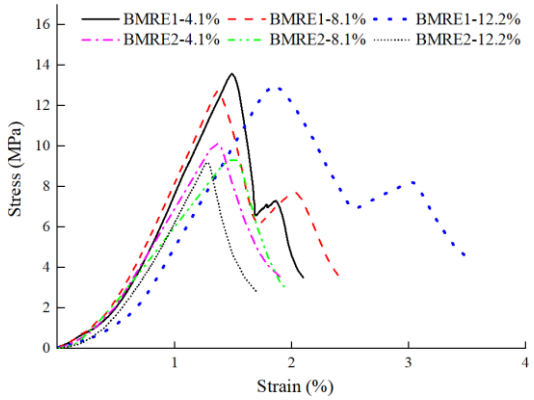

Fig. 10 Stress-strain curves of different block volumetric block proportio

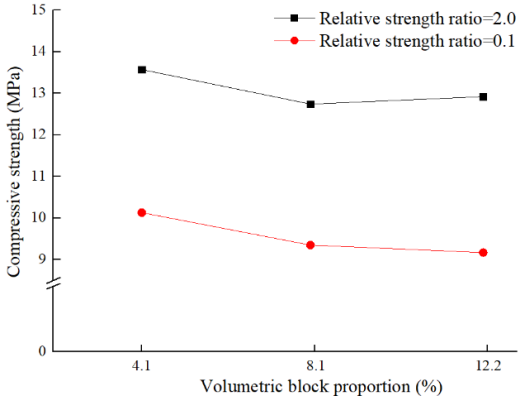

Fig. 11 The relationship between volumetric proportion and reinforcement strength

strength increases with increase in volumetric block proportion. The stress-strain curves (BMRE2) are all unimodal and similar to the above-mentioned stress-strain curve of BMRC37. It can be seen from the stress-strain curves that the overall strength of the reinforced samples is affected by the volumetric block proportion.

Fig. 11 shows the influence of the volumetric block proportion under different relative strength ratios (λ) on the reinforcement strength. When λ=2.0 (BMRE1), reinforcement strength first decreases and then increases the increase in volumetric block proportion; when λ=0.1 (BMRE2), reinforcement strength gradually decreases with increase in volumetric block proportion. The reasons are as follows: when λ>1, the interface strength is weaker relative to the strength of mortar specimens and cement-based grout stone body. While increased volumetric block proportion strengthens skeleton support for the reinforced broken rock sample, at the same time the weak areas in the reinforced sample also increase, which in turn reduces the strength of the sample. Therefore, when λ>1 the volumetric block proportion has both positive and negative effects on strength: the final result depends on the relative effect of the interface strength and the strength of the rock block. When λ<1 the increase in the volumetric block proportion of rock block is equivalent to replacing the cement-based grout stone body with higher strength. The result is that the content of cement-based grout stone body is reduced, thereby reducing the overall strength of the reinforcement,

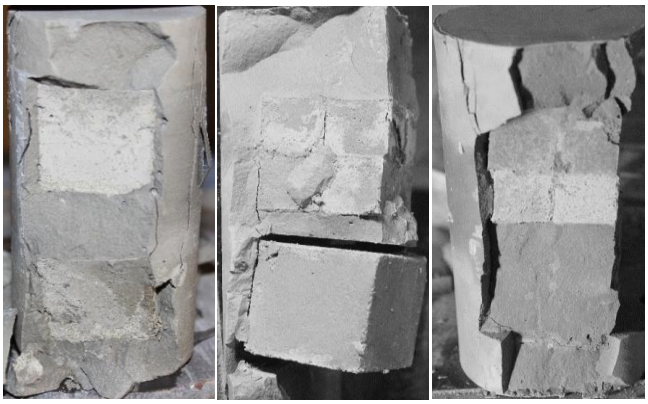

(a) BMRC32*2 (b) BMRC11*8 and BMRC32 (c) BMRC11*16

Fig. 12 Internal failure of reinforced samples with different degrees of fragmentation (λ=2.0)

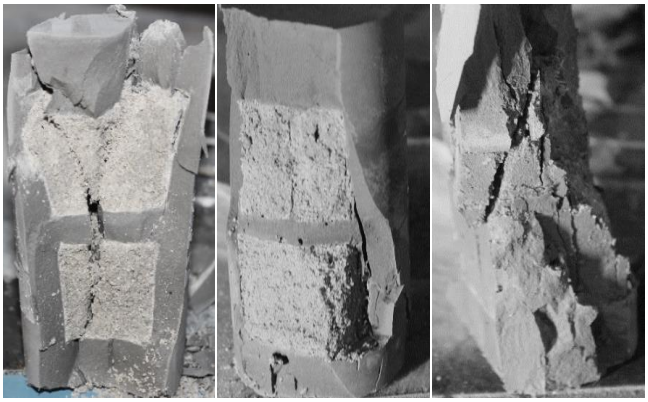

(a) BMRC37*2 (b) BMRC12*8 and BMRC37 (c) BMRC12*16

Fig. 13 Internal failure of reinforced samples with different degrees of fragmentation (λ=0.1)

and increase in interface further reduces the overall strength of the reinforcement. Therefore, when λ<1 the volumetric block proportion only has a negative effect on reinforcement strength, and the reinforcement strength decreases with increase in volumetric block proportion.

3.3 The influence of degree of fragmentation on the strength of reinforced broken rock mass

3.3.1 Mode of reinforcement failure

Fig. 12 shows the uniaxial compression test results for the reinforced samples (BRMC11 and BRMC32) with different degrees of fragmentation. The integrity of the mortar specimens is good, and failure is mainly interface failure. Fig. 13 shows the uniaxial compression test results of the reinforced samples (BRMC12 and BRMC37) with different degrees of fragmentation. The cracks are generated inside the mortar specimens, and failure is mainly specimen failure.

3.3.2 Stress-strain curves

Fig. 14 shows the stress-strain curves of the reinforcement samples with mortar specimens of different degrees of fragmentation. It can be seen that the stress-strain curves (BMRC32, BMRC11 and BMRC32, BMRC11) are all bimodal, the second peak strength decreases with the increase of degree of fragmentation. And the stress-strain curves (BMRC37, BMRC12 and BMRC37, BMRC12) are all unimodal.

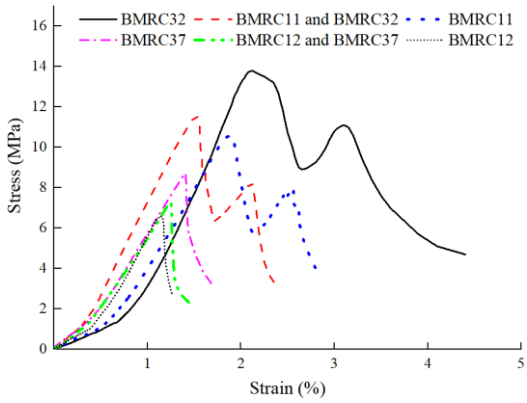

Fig. 14 Stress-strain curves with different degrees of fragmentation

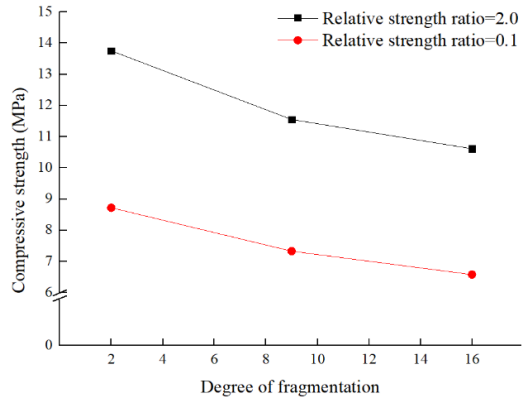

Fig. 15 The relationship between degree of fragmentation and reinforcement strength

Overall reinforcement strength is affected by the degree of fragmentation. Fig. 15 shows the influence of degree of fragmentation under different relative strength ratios (λ) on reinforcement strength. Under the condition of certain volumetric block proportion, as the degree of fragmentation increases, the overall strength of reinforcement gradually decreases. Relative strength ratio only affects peak strength and has nothing to do with the overall trend of the curve, indicating that the degree of fragmentation has a negative effect on overall strength of the reinforcement.

3.4 The influence of shape on the strength of reinforced broken rock mass

3.4.1 Mode of reinforcement failure

Fig. 16 shows the uniaxial compression test results of the reinforced samples (BRMS1, BRMC21 and BRME1) with different shapes. The integrity of the mortar specimens is good, and failure is mainly interface failure. Fig. 17 shows the uniaxial compression test results of the reinforced samples (BRMS2, BRMC22 and BRME2) with different shapes. The cracks are generated inside the mortar specimens, and failure is mainly specimen failure.

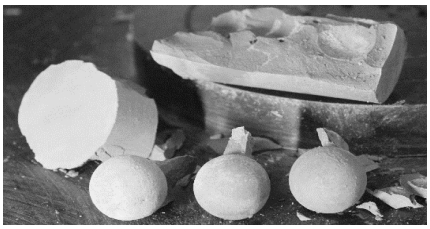

(a) BRMS1

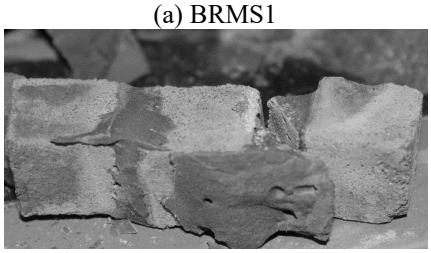

(b) BRMC21

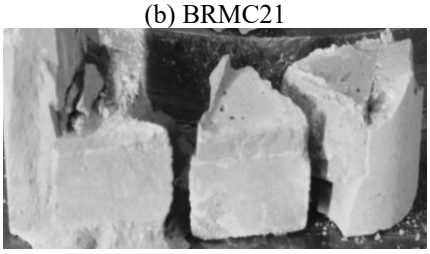

(c) BRME1

Fig. 16 Internal failure of reinforced samples with different shapes (λ=2.0)

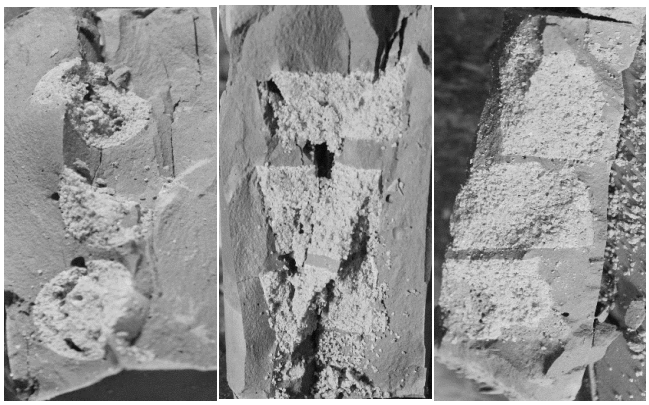

(a) BMR2 (b) BMRC22 (c) BRME2

Fig. 17 Internal failure of reinforced samples with different shapes (λ=0.1)

3.4.2 Stress-strain curves

Fig. 18 shows the stress-strain curves of the reinforced samples with mortar specimens of different shapes. The stress-strain curves (BRMS1, BRMC21, BRME1) are all bimodal, and the stress-strain curves (BRMS2, BRMC22, BRME2) are all unimodal. From Fig. 18, it can be considered that the overall trend of the stress-strain curve is related to relative strength ratio, not to the shape of the rock block.

The overall strength of reinforcement is affected by the shape of the rock block. Fig. 19 shows the influence of these shapes under different relative strength ratios (λ) on reinforcement strength. The shape of internal rock blocks of different strength has a different influence on the strength of reinforcement. When λ=2.0, reinforcement strength of the

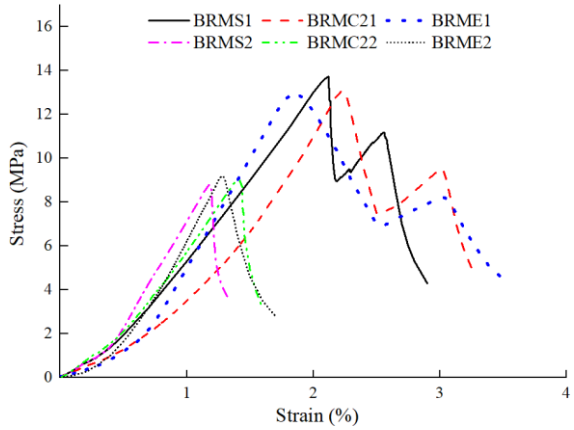

Fig. 18 Stress-strain curves with different Shapes

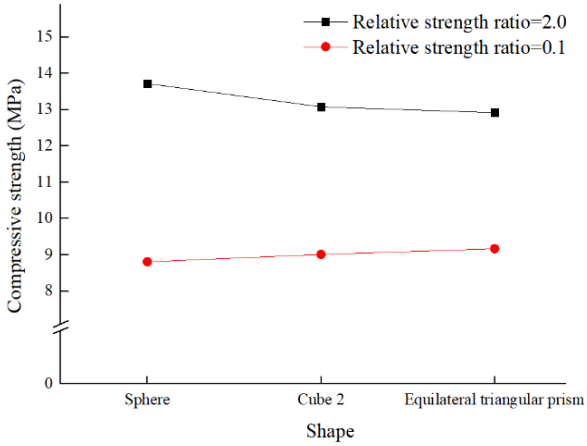

Fig. 19 The relationship between shape and reinforcement strength

sphere is greater than that of the cube which in turn is greater than that of the equilateral triangular prism; that is, reinforcement strength increases with increase in sphericity.

The opposite results when λ=0.1: the reinforcement strength of the sphere is less than that of the cube which in turn is less than that of the equilateral triangular prism. That is, reinforcement strength decreases with increase in sphericity. There are two reasons for the difference: (1) the difference in shape of the rock block will lead to anisotropy of the reinforced sample, and under the action of load, the phenomenon of stress concentration occurs in the internal interface (Romanova *et al.* 2009, Binaree *et al.* 2020). When λ>1, the interface is the main factor that controls the failure of reinforcement strength. Compared with the sphere, the cube and triangular prism have edges and corners, and the phenomenon of stress concentration is more likely to occur at the edges, which makes the interface more vulnerable to damage; (2) different shapes of rock block have different cementation modes. When the volume of the rock blocks is the same, the effective cementation area of the angular rock block is larger than that of the spherical rock block. When λ<1, cementation of the interface will promote reinforcement strength. At the same time, weakened rock blocks increase the tortuosity of failure surface with increase in angularity, that is, the friction effect can also promote reinforcement strength.

4. Discussion

The overall mechanical properties of reinforced broken rock mass are not only affected by the strength, degree of fragmentation, and shape of broken rock mass, but also by the mechanical properties of slurry materials, the strength difference between broken rock mass and cement-based grout stone body, and the volumetric block proportion of the broken rock mass in the reinforcement. However, because of the complexity of the broken rock mass structure in underground engineering, it is very difficult to study the influence of these various factors on the strength of reinforced broken rock mass. The method of laboratory testing of artificial samples is simple to operate, involves easy-to-control variables, and has strong test repeatability. As such, it provides a new way of studying the influence of various factors on the strength of reinforcement.

The research in this study shows that except for degree of fragmentation, relative strength ratio (λ) is the main factor affecting the variation of the strength characteristics of reinforcement. For λ>1 and λ<1, the various factors have opposite influences on reinforcement strength. It is generally believed that for λ>1, the strength of reinforced broken rock mass gradually increases with increase in volumetric block proportion of broken rock mass (Howarth and Rowlands 1987, Burgi *et al*. 2001). However, in this paper, the strength of reinforcement decreases first and then increases with increase in volumetric block proportion. The reason is that existing research uses broken rock mass with volumetric block proportion greater than 15% as the research object, and not those cases of smaller volumetric block proportion. For broken rock mass with volumetric block proportion greater than 15%, the results in this paper confirm those in the existing literature.

This study looked at the influence of the relative strength ratio, volumetric block proportion, degree of fragmentation, and shape of different rock blocks on the macroscopic characteristics of reinforced broken rock mass. However, it should be pointed out that: The shape of natural broken rock mass is different, it is impossible to make up of the same rock blocks in the reinforcement, and there may be fillers between rock blocks. Consideration should be given to the influence of fillers on the strength characteristics of reinforced broken rock mass that has fillers. In addition, given that the spatial distribution of broken rock mass is random, it is necessary to carry out further research on the spatial distribution characteristics of broken rock mass.

5. Conclusions

In this study, a series of experimental studies were carried out to investigate the influence of a range of critical factors (e.g., strength and volume of cement-based grout stone body and characteristics of broken rock mass). The following are some major findings:

• The relative strength ratio between the broken rock mass and cement-based grout stone body (λ) plays an important role in governing the strength and deformation of the reinforced broken rock mass. A higher λ could generally lead to better reinforcement outcomes. Importantly, the influence of the volumetric block proportion (VBP) of rock block on the reinforcement strength is related to λ. When λ <1, the increase of VBP could decrease the mechanical strength of the reinforced broken rock mass.

• The compressive strength of grouting reinforced broken rock mass generally decreases with the increase of the degree of fragmentation.

• Under a relatively high strength ratio (e.g., λ=2.0), the enhancement in compressive strength by grouting is more obvious for broken rock mass with spherical shape, whereas the shape of rock mass has little influence when the strength ratio is low (e.g., λ=0.1).

• The experimental results show that the failure mode of reinforced broken rock mass can be grouped into two typical failure modes (i.e., columnar splitting failure and inclined shear failure) which depend on the strength and structure of the broken rock mass. In addition, the failure process can be roughly characterized as occurring in four stages: compaction stabilization stage, linear elasticity stage, plastic stage, and failure stage.

Acknowledgements

The research described in this paper was financially supported by the Joint Funds of National Natural Science Foundation of China [grant number U1706223], the China Scholarship Council [file number 201906220133], the National Natural Science Foundation of China [grant number 52109131], and the Natural Science Foundation of Shandong Province [grant number ZR2020QE290].

References

Afifipour, M. and Moarefvand, P. (2014), "Mechanical behavior of bimrocks having high rock block proportion", *Int. J. Rock Mech. Min. Sci.*, **65**, 40-48. https://doi.org/10.1016/j.ijrmms.2013.11.008.

Agustawijaya, D.S. (2007), "The uniaxial compressive strength of soft rock", *Civil Engineering Dimension*, **9**(1), 9-14. https://doi.org/10.9744/ced.9.1.pp.%209-14.

Alber, M. and Kahraman, S. (2009), "Predicting the uniaxial compressive strength and elastic modulus of a fault breccia from texture coefficient", *Rock Mech. Rock Eng.*, **42**(1), 117-127. https://doi.org/10.1007/s00603-008-0167-x.

Asadizadeh, M., Hossaini, M.F., Moosavi, M., Masoumi, H. and Ranjith, P.G. (2019), "Mechanical characterisation of jointed rock-like material with non-persistent rough joints subjected to uniaxial compression", *Eng.Geol.*, **260**, 105224. https://doi.org/10.1016/j.enggeo.2019.105224.

Avşar, E. (2020), "Contribution of fractal dimension theory into the uniaxial compressive strength prediction of a volcanic welded bimrock", *Bull. Eng. Geol. Environ.*, **79**(7), 3605-3619. https://doi.org/10.1007/s10064-020-01778-y.

Binaree, T., Azéma, E., Estrada, N., Renouf, M. and Preechawuttipong, I. (2020), "Combined effects of contact friction and particle shape on strength properties and microstructure of sheared granular media", *Phys. Rev. E*, **102**(2), 022901. https://doi.org/10.1103/PhysRevE.102.022901.

Brown, E.T. (1981), *Rock Characterization Testing and Monitoring*, Oxford: Pergamon Press.

https://doi.org/10.1016/0148-9062(81)90524-6.

Bürgi, C., Parriaux, A. and Franciosi, G. (2001), "Geological characterization of weak cataclastic fault rocks with regards to the assessment of their geomechanical properties", *Q. J. Eng. Geol. Hydroge.*, **34**(2), 225-232. https://doi.org/10.1144/qjegh.34.2.225.

Coli, N., Berry, P. and Boldini, D. (2011), "In situ non-conventional shear tests for the mechanical characterisation of a bimrock", *Int. J. Rock Mech. Min. Sci.*, **48**(1), 95-102. https://doi.org/10.1016/j.ijrmms.2010.09.012.

Fereshtenejad, S., Kim, J. and Song, J. J. (2021), "Empirical Model for Shear Strength of Artificial Rock Containing a Single Nonpersistent Joint", *Int. J. Geomech.*, **21**(8), 04021123. https://doi.org/10.1061/(ASCE)GM.1943-5622.0002099.

Gerolymatou, E. and Triantafyllidis, T. (2016), "Shearing of materials with intermittent joints", *Rock Mech. Rock Engi.*, **49**(7), 2689-2700. https://doi.org/10.1007/s00603-016-0956-6.

Ghareh, S., Kazemian, S. and Shahin, M. (2020), "Assessment of compressibility behavior of organic soil improved by chemical grouting: An experimental and microstructural study", *Geomech. Eng.*, **21**(4), 337-348. https://doi.org/10.12989/gae.2020.21.4.337.

Goodman, R.E. and Ahlgren, C.S. (2000), "Evaluating safety of concrete gravity dam on weak rock: Scott Dam", *J. Geotech. Geoenviron. Eng.*, **126**(5), 429-442. https://doi.org/10.1061/(ASCE)1090-0241(2000)126:5(429).

Guo, Y.X., Zhang, Q.S., Xiao, F., Liu, R.T., Wang, Z.J. and Liu, Y.K. (2020), "Grouting rock fractures under condition of flowing water", *Carbonates and Evaporites*, **35**(3), 1-15. https://doi.org/10.1007/s13146-020-00619-z.

Guo, Y.X., Zhang, Q.S., Zhang, L.Z., Liu, R.T., Chen, X. and Liu, Y.K. (2021), "Experimental study on groutability of sand layer concerning permeation grouting", *Adv. Mater. Sci. Eng.*, **2021**, 1-10. https://doi.org/10.1155/2021/6698263.

Howarth, D.F. and Rowlands, J.C. (1987), "Quantitative assessment of rock texture and correlation with drillability and strength properties", *Rock Mech. Rock Eng.*, **20**(1), 57-85. https://doi.org/10.1007/BF01019511.

Huang, M., Xu, C.S., Zhan, J.W. and Wang, J.B. (2017), "Comparative study on dynamic properties of argillaceous siltstone and its grouting-reinforced body", *Geomech. Eng.*, **13**(2), 333-352. https://doi.org/10.12989/gae.2017.13.2.333.

Jin, Y.H., Han, L.J., Meng, Q.B., Ma, D., Wen, S.Y. and Wang, S. (2018), "Experimental investigation of the mechanical behaviors of grouted crushed coal rocks under uniaxial compression", *Geomech. Eng.*, **16**(3), 273-284. https://doi.org/10.12989/gae.2018.16.3.273.

Johnston, I.W. and Choi, S.K. (1986), "A synthetic soft rock for laboratory model studies", *Geotechnique*, **36**(2), 251-263. https://doi.org/10.1680/geot.1986.36.2.251.

Kahraman, S. and Alber, M. (2006), "Estimating unconfined compressive strength and elastic modulus of a fault breccia mixture of weak blocks and strong matrix", *Int. J. Rock Mech. Min. Sci.*, **43**(8), 1277-1287. https://doi.org/10.1016/j.ijrmms.2006.03.017.

Kalender, A.Y.C.A.N., Sonmez, H., Medley, E., Tunusluoglu, C. and Kasapoglu, K.E. (2014), "An approach to predicting the overall strengths of unwelded bimrocks and bimsoils", *Eng. Geol.*, **183**, 65-79. https://doi.org/10.1016/j.enggeo.2014.10.007.

Kim, K.Y., Suh, H.S., Yun, T.S., Moon, S.W. and Seo, Y.S. (2016), "Effect of particle shape on the shear strength of fault gouge", *Geosci. J.*, **20**(3), 351-359. https://doi.org/10.1007/s12303-015-0051-0.

Li, Y., Huang, R., Chan, L.S. and Chen, J. (2013), "Effects of particle shape on shear strength of clay-gravel mixture", *KSCE J. Civil Eng.*, **17**(4), 712-717. https://doi.org/10.1007/s12205-013-0003-z.

Li, Z., Wang, Y.H., Ma, C.H. and Mok, C.M.B. (2017), "Experimental characterization and 3D DEM simulation of bond breakages in artificially cemented sands with different bond strengths when subjected to triaxial shearing", *Acta Geotechnica*, **12**(5), 987-1002. https://doi.org/10.1007/s11440-017-0593-6.

Liu, G., Feng, X.T., Jiang, Q., Yao, Z. and Li, S. (2017), "In situ observation of spalling process of intact rock mass at large cavern excavation", *Eng. Geol.*, **226**, 52-69. https://doi.org/10.1016/j.enggeo.2017.05.012.

Liu, Z., Zhou, C., Lu, Y., Yang, X., Liang, Y. and Zhang, L. (2018), "Application of FRP bolts in monitoring the internal force of the rocks surrounding a mine-shield tunnel", *Sensors*, **18**(9), 2763.https://doi.org/10.3390/s18092763.

Liu, Z., Zhou, C., Su, D., Du, Z., Zhu, F. and Zhang, L. (2019), "Rheological deformation behavior of soft rocks under combination of compressive pressure and water-softening effects", *Geotech. Test. J.*, **43**(3), 737-757. https://doi.org/10.1520/GTJ20180342.

Mahdevari, S. and Moarefvand, P. (2018), "Experimental investigation of fractal dimension effect on deformation modulus of an artificial bimrock", *Bull. Eng. Geol. Environ.*, **77**(4), 1729-1737. https://doi.org/10.1007/s10064-017-1074-8.

Mahdevari, S., Moarefvand, P. and Mohammadzamani, D. (2020), "Considering the effect of block-to-matrix strength ratio on geomechanical parameters of bimrocks", *Geotech. Geol. Eng.*, **38**(5), 4501-4520. https://doi.org/10.1007/s10706-020-01304-7.

Ozturk, C.A. and Nasuf, E. (2013), "Strength classification of rock material based on textural properties", *Tunn. Undergr. Sp. Tech.*, **37**, 45-54. https://doi.org/10.1016/j.tust.2013.03.005.

Romanova, V.A., Balokhonov, R.R. and Schmauder, S. (2009), "The influence of the reinforcing particle shape and interface strength on the fracture behavior of a metal matrix composite", *Acta Materialia*, **57**(1), 97-107. https://doi.org/10.1016/j.actamat.2008.08.046.

Sagong, M., Choi, I.Y., Lee, J.S. and Cho, C.S. (2020), "Shear strength behaviors of grouts under the blasting induced vibrations", *Geomech. Eng.*, **21**(2), 207-213. https://doi.org/10.12989/gae.2020.21.2.207.

Savely, J.P. (1990), "Determination of shear strength of conglomerates using a caterpillar D9 ripper and comparison with alternative methods", *Int. J. Min. Geol. Eng.*, **8**(3), 203-225. https://doi.org/10.1007 / BF01554042.

Shakeri, M.R., Haeri, S.M., Shahrabi, M.M., Khosravi, A. and Sajadi, A.A. (2018), "An experimental study on mechanical behavior of a calcite cemented gravelly sand", *Geotech. Test. J.*, **41**(3), 494-507. https://doi.org/10.1520/GTJ20170095.

Shaunik, D. and Singh, M. (2019), "Strength behaviour of a model rock intersected by non-persistent joint", *J. Rock Mech. Geotech. Eng.*, **11**(6), 1243-1255. https://doi.org/10.1016/j.jrmge.2019.01.004.

Shen, B. (2014), "Coal mine roadway stability in soft rock: a case study", *Rock Mech. Rock Eng.*, **47**(6), 2225-2238. https://doi.org/10.1007/s00603-013-0528-y.

Sonmez, H., Ercanoglu, M., Kalender, A.Y.C.A.N., Dagdelenler, G. and Tunusluoglu, C. (2016), "Predicting uniaxial compressive strength and deformation modulus of volcanic bimrock considering engineering dimension", *Int. J. Rock Mech. Min. Sci.*, **100**(86), 91-103. https://doi.org/10.1016/j.ijmms.2016.03.022.

Ulusay, R. and Erguler, Z.A. (2012), "Needle penetration test: evaluation of its performance and possible uses in predicting strength of weak and soft rocks", *Eng. Geol.*, **149-150**, 47-56. https://doi.org/10.1016/j.enggeo.2012.08.007.

Xiao, Y., Yuan, Z., Lin, J., Ran, J., Dai, B., Chu, J. and Liu, H. (2019), "Effect of particle shape of glass beads on the strength and deformation of cemented sands", *Acta Geotechnica*, **14**(6),

2123-2131. https://doi.org/10.1007/s11440-019-00830-w.

Zhang, B., Li, S.C., Yang, X.Y., Xia, K.W., Liu, J.Y., Guo, S. and Wang, S.G. (2019), "The coalescence and strength of rock-like materials containing two aligned X-type flaws under uniaxial compression", *Geomech. Eng.*, **17**(1), 47-56. https://doi.org/10.12989/gae.2019.17.1.047.

Zhang, Y., Jiang, Y., Asahina, D. and Wang, C. (2020), "Experimental and numerical investigation on shear failure behavior of rock-like samples containing multiple non-persistent joints", *Rock Mech. Rock Eng*., **53**(10), 4717-4744. https://doi.org/10.1007/s00603-020-02186-0.

Zhou, C.Y., Lu, Y.Q., Liu, Z. and Zhang. L.H. (2019), "An innovative acousto-optic-sensing-based triaxial testing system for rocks", *Rock Mech. Rock Eng.*, **52**(9), 3305-3321. https://doi.org/10.1007/s00603-019-01764-1.

Zhou, C.Y., Yu, L.F., You, F., Liu, Z., Liang, Y.H. and Zhang. L.H. (2020a), "Coupled seepage and stress model and experiment verification for creep behavior of soft rock", *Int. J. Geomech.*, **20**(9), 04020146. https://doi.org/10.1061/(ASCE)GM.1943-5622.0001774.

Zhou, X.P., Bi, J., Deng, R.S. and Li, B. (2020b), "Effects of brittleness on crack behaviors in rock-like materials", *J. Test. Eval.*, **48**(4), 2829-2851. https://doi.org/10.1520/JTE20170595.

CC